

# Forecasting Extreme Day and Night Heat in Paris\*

Richard Berk  
University of Pennsylvania

August 26, 2025

## Abstract

As a demonstration of concept, quantile gradient boosting is used to forecast diurnal and nocturnal  $Q(.90)$  air temperatures for Paris, France during late the spring and summer months of 2020. The data are provided by the Paris-Montsouris weather station.  $Q(.90)$  values are estimated because the 90th percentile requires that the temperatures be relatively rare and extreme. Predictors include seven routinely collected indicators of weather conditions, lagged by 14 days; the temperature forecasts are produced two weeks in advance. Conformal prediction regions capture forecasting uncertainty with provably valid properties. For both diurnal and nocturnal temperatures, forecasting accuracy is promising, and sound measures of uncertainty are provided.

**Keywords**— heat waves, forecasting, quantile gradient boosting, quantile regression forests, conformal prediction regions

---

\*Arun Kuchibhotla provided very helpful feedback on the discussion of conformal prediction regions.

# 1 Introduction

There has long been an interest in anthropogenic global warming (Schneider, 1989) and more recently, its associated increase in the frequency and intensity of heat waves (Tziperman, 2022, chap. 13). One implication is that accurate forecasts of rare, high temperatures can have significant benefits for subject-matter understanding and policy preparedness. There are data analysis and simulation methods that can help, but they can be demanding to implement and can struggle at the smaller spatial scales when such forecasts are needed. Valid estimates of uncertainty also can be lacking.

In this paper, temperature forecasting is undertaken with quantile machine learning and conformal prediction regions easily applied to weather station data.  $Q(.90)$  diurnal and nocturnal temperatures are forecasted with promising accuracy and valid estimates of forecasting uncertainty. The approach perhaps can be seen as a complement to the “industrial strength” methods that seem to dominate the literature.

Section 2 briefly provides some background. Section 3 describes the data and forecasting methods. Section 4 presents the  $Q(.90)$  temperature forecasts with conformal prediction regions. Section 5 is a discussion of the results and their possible implications for future work. Conclusions are drawn in Section 6.

## 2 Background

Unusually high temperatures have become a prominent research topic (Perkins, 2015; Piticar et al., 2019; Marx et al., 2021; Klingelhöfer et al., 2023; IPCC, 2023; Guimarães et al., 2024). Description and explanation dominate the enterprise (Mann et al., 2018; Petoukhov et al., 2013; McKinnon and Simpson, 2022; Li et al., 2024). Forecasting rare and extreme temperatures is too often ignored or addressed as an afterthought. As a case in point, numerical weather prediction can include heat wave forecasts, but with curious uncertainty estimates (Fu, 2025) and chiefly as a subordinate feature of large weather system analyses (Pu and Kalnay, 2018; Harper, 2024).

There are some recent studies that begin to right the balance. At Microsoft and at Deep Mind, impressive “AI” tools have been built that can forecast extreme weather events, but those weather events do not yet center on exceptional heat (Price et al., 2024; Bodnar et al., 2025). Jacques-Dumas et al. (2022) forecast “long lasting heat waves” with as much as a 15 day lead time. Output from a climate simulation is provided to a convolution neural network in which the rare heat wave events are upweighted. However, upweighting is an analogue to choice based sampling that can badly compromise any accuracy claims (Manski and Lerman, 1977). Miloshevich et al. (2024) undertake a forecasting methods comparison between a stochastic weather generator (i.e. essentially a Markov Chain) and convolutional neural networks using 80 batches of general circulation model (GCM) output, each of 100 years. The primary goal is to forecast 15 day heat waves. There are great many details based on somewhat discretionary decisions making general conclusions problematic, but the CNN approach is declared the winner.

Forecasting studies relying on “AI” tools often address very challenging subject-matter and

research methods that make it easy to quibble. Yet, some difficulties can be fundamental. De rigueur deep neural networks, for instance, can in principle improve extreme heat forecasting accuracy, but as some commentators note, “The configuration and design of artificial deep neural networks is error prone, time consuming and difficult” (Galván and Mooney, 2021, 2). In response, there are various kinds of auxiliary algorithms, sometimes based on reinforcement learning, whose job is to help specify desirable neural network architectures (Elsken et al., 2019). These network specification approaches have promise but overlay additional code burdened by its own technical challenges. There also are concerns about the resources consumed to train enormous neural networks. Often, many CPUs and/or GPUs housed in “server farms” are required, managed by a substantial number of software engineers. Further, improvements in accuracy at larger scales can be compromised when applied at smaller scales having substantial spatial variation across different topographical settings (e.g., London, versus Winnipeg versus Riyadh). There is great difficulty, as well, obtaining valid estimates of uncertainty.

Forecasts resting on climate simulation output rely on different theoretical foundations and mathematical methods. Despite some remarkable accomplishments, they can fall victim to related concerns. The Community Earth System Model (CESM), for example, seems ill equipped to address rare and extreme heat, especially at the small spatial scales required. Evaluations of downscaling methods are mixed. Recent research suggests that deep learning might improve downscaling (Wang et al., 2021), but once again, there is a new and complicated overlay. Data assimilation can improve large scale modeling performance, but is not a downscaling method. Finally, properly accounting for uncertainty remains problematic. “Uncertainty in climate models has several components. They are related to the model itself, to the initial conditions of the model...and to the inputs that affect the model... All three must be addressed for the model to be useful” (Gettleman and Rood, 2016, 12). For these reasons and others, one must be cautious about treating model simulation output as if it were real data.

The mechanisms creating extreme heat are increasingly understood (Tziperman, 2022, chap. 13). But for both large scale “AI” methods and climate simulations, forecasting the presence or absence heat waves, rather than high temperatures, can be a distraction (Smith et al., 2013). Perkins and Alexander (2013, 1) caution, “... definitions and measurements of heat waves are ambiguous and inconsistent, generally being endemic to only the group affected, or the respective study reporting the analysis.” Moreover, heat wave definitions can be media driven (Hulme et al., 2008; Hopke, 2020). Noteworthy heat is newsworthy heat. In short, it can be risky to treat heat waves as discrete statistical events when the reality is far more nuanced and challenging to measure.

Finally, the role of excessive nocturnal heat commonly is overlooked. Yet, high nocturnal temperatures can significantly threaten local ecosystems and public health. Critical recovery time from excessive daytime temperatures can be sacrificed (Walther et al., 2002; Anderson and Bell, 2009; He et al., 2022). Nocturnal temperatures are easy to overlook because they are almost never the highest daily temperatures. In addition, they are shaped by somewhat different mechanisms than diurnal temperatures.

In the pages ahead, forecasts of local, extreme and high temperatures are the topic, both during the day and at night. Quantile supervised learning and conformal prediction inference are the main

tools. They are applied to weather station data. Promising results are achieved.

### 3 Data and Methods

The data come from the Paris-Montsouris weather station. Observations from 2020 are employed for training. A temporal index  $t = 1, 2, 3, \dots, T$  denotes each of 183 days from March 1st to September 30th used in the analysis. The two response variables are centigrade air temperatures at 2PM and 2AM solar time. These solar times serve as proxies for the warmest daily diurnal and nocturnal temperatures, which are not necessarily the most extreme heat day after day. Solar time provides a useful and consistent time stamp for the analyses while avoiding local conventions such as the presence or absence of daylight savings time.

Paris is chosen because of its reputation for respecting science and scientific data free of political meddling. Any of several other locales could have been selected and will be in future work. At the moment, Paris may be Europe’s urban, high temperature ground zero (Porter, 2025). Measured temperatures rather than Steadman heat index values are favored for the response variables because of well known problems with the index at temperatures less than 80°F (Steadman, 1979; Rothfus, 1990). Such temperatures are common in Paris after dark during the summer months.

Predictors *lagged by 14 days* include (1) wind direction in degrees from true north, (2) wind speed in meters per second, (3) air temperature in degrees celsius, (4) atmospheric pressure in hectopascals (hPa), (5) visibility in meters, (6) dew point in degrees celsius, (7) relative humidity in percent units, and (8) a counter for the day ranging from 1 to 183 days. The counter is included to account for warming trends from early to late summer. One would expect that on the average, early August will be warmer than early June, although the increases can be nonlinear over time. At least some of these variables are likely to be related to well-known precursors of heat waves such as dry soil, the absence of clouds, and elevated barometric pressure in the mid-troposphere functioning together as high order interaction effects with routine seasonal warming (Tziperman, 2022, chap. 13). Data from each of the last 15 days in March are included solely to obtain the values of the lagged predictors for each the pertinent days in April two weeks later.

Because of the data’s longitudinal structure, temporal dependence can be an important complication. Test data cannot be obtained by random sampling without scrambling time series dependence (Hyndman and Athanasopoulos, 2021, sec. 5.8). As an alternative, test data are drawn from Paris-Montsouris weather station from March 1st to September 30th 2021. The same thermodynamics and other physical processes should apply during the identical months in 2020 and 2021, although there can be significant random variation in the realized data.

There can be some subtle issues. Important predictors can be in very different regions of the predictor space in different seasons. With strong nonlinear relationships (Stull, 2017, chap. 3), predictor values may fall at relatively flat parts of the response function in winter and at relatively steep parts of the response function in the summer (or vice versa). Yet the response function is the same. As an empirical matter, this might look like a change in the response function itself. Because forecasting, not explanation, is the intent, such complications can be overlooked for now. Moreover, an algorithm is not a model (Breiman, 2001). As Kearns and Roth (2019, 4) emphasize, “But first,

what is an algorithm anyway? At its most fundamental level, an algorithm is nothing more than a very precisely specified series of instructions for performing some concrete task.”

The multiple time series observations are analyzed with quantile gradient boosting (Friedman, 2001, 2002) using a .90 quantile estimation target to focus on extreme and rare high temperatures (Velthoen et al., 2023). Using quantiles also has the indirect benefit of bypassing the need explicitly to take into account the full temperature distribution when rare, high temperatures are defined. A loess smoother provides visual summaries as needed. Adaptive conformal prediction regions are estimated by quantile random forests (Meinshausen, 2006; Romano et al., 2019) because quantile gradient boosting aborted on this task after one iteration. The rationales for using these procedures are presented later in the grounded context of specific results. Pseudocode is provided as part of that discussion.

## 4 Results

### 4.1 Response Variable Descriptive Statistics

Figure 1 displays on the left, a histogram of 2PM celsius, air temperatures with a generalized extreme value (GEV) distribution overlaid. The right histogram provides the same information of the 2AM celsius temperatures. Both histograms look rather symmetric and lack the long right tail emblematic of the GEV distribution. The 2PM temperatures tend to show higher values, just as one should expect. They have a 2PM  $Q(.90)$  value of approximately  $30^{\circ}\text{C}$ . The 2AM  $Q(.90)$  value is approximately  $20^{\circ}\text{C}$ .

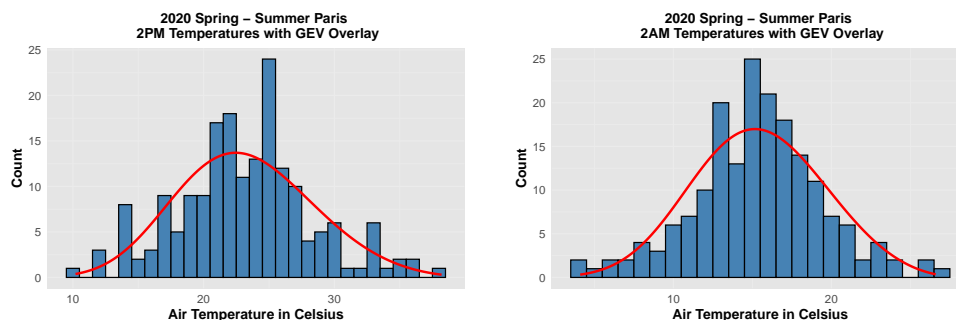


Figure 1: Histograms with GEV distribution overlays of the Paris Daily 2PM and 2AM Air temperatures in Celsius for April through September in 2020 ( $N = 183$  days)

The .90 quantile is a provisional way to define “rare.” It represents a compromise between a focus on atypical temperatures and the need for regions in the predictor space to contain sufficient data. For both distributions, their right tails include several relatively unusually high temperatures. None appear as obvious outliers. They illustrate some possible forecasting targets, but are from marginal distributions. Conditional distributions are needed as the foundation for forecasts.

## 4.2 Fitting Quality

Fitting the  $Q(.90)$ , 2PM temperatures with quantile gradient boosting implies an asymmetric loss function that incentivizes the boosting algorithm to weight underestimates far more heavily than overestimates. In the following quantile loss function,  $\tau = .90$ ; underestimates are 9 times more costly to the loss than overestimates.

$$L_\tau(y, \hat{y}) = \begin{cases} \tau \cdot (y - \hat{y}) & \text{if } y \geq \hat{y} \\ (1 - \tau) \cdot (\hat{y} - y) & \text{if } y < \hat{y}. \end{cases} \quad (1)$$

The left display on Figure 2 is a plot of the 2020 observed 2PM celsius temperatures against the 2020 2PM fitted  $Q(.90)$  celsius temperatures. The values for each day are in red, the blue line is a loess smooth serving as a visual aid, and the gray band is a conventional prediction error band. Because the requisite assumptions are not met, the prediction error band is just a representation of some customary practice. For example, temporal dependence is ignored. A better approach is used later.

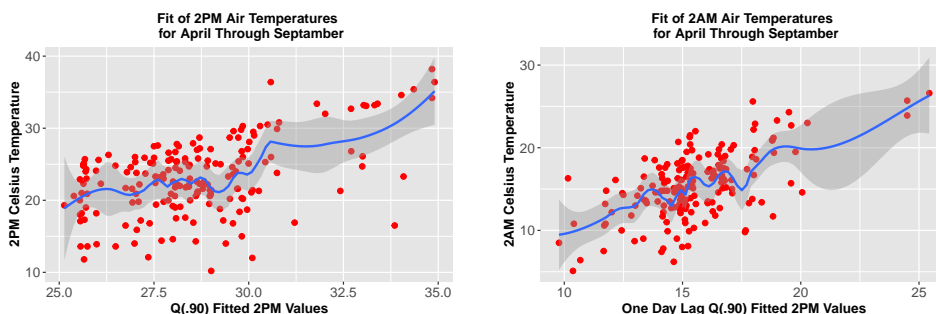


Figure 2: Fit quality for quantile gradient boosting applied to the 2020 daily Paris 2PM results on the left and 2020 daily Paris 2AM results on the right. For both, the red dots are the observations, the red line is a loess smooth, and the gray band is a conventional prediction error band. ( $N = 183$  days)

It is important to recall that the fitted values result from the trained quantile boosting algorithm with all eight predictors measured two weeks earlier. That is, conditional on the 8 predictors, the 90th percentile of the afternoon temperatures is anticipated 14 days in advance. The 14 days lag is perhaps a plausible upper bound at which instructive temperature forecasts can be made. It has been used before to study heat waves (Li et al., 2024).<sup>1</sup>

The right display on Figure 2 is a plot of the observed 2020 2AM celsius temperatures against the 2020 2PM *fitted*  $Q(.90)$  celsius temperatures lagged by one day. The 14 day lagged 2AM

<sup>1</sup>The gbm procedure in R was used. The shrinkage value was specified as 0.0001 to encourage slow improvements over iterations. The rationale was to capture relatively rare events. To further that goal, an interaction depth of 6 was used with a minimum node size of 5. The software iterated through 100,000 boosted regression trees and settled on 28,233 as the appropriate number using performance in the test data as a criterion. On a Macintosh Studio desktop, the 100,000 sequential trees were computed in well under 5 seconds in real time.

predictors were essentially unrelated to the 2AM observed temperatures. This is no surprise. High temperatures are substantially driven by solar radiation. At night, the sun is below the horizon. But there is thermal inertia through which air warmed during the day retains some of the heat that night. A good predictor of 2AM temperatures should be the *fitted* 2PM temperatures 12 hours earlier (i.e., for daily data, nominally a one day lag). The *observed* 2PM temperatures from the day before cannot be used for forecasting in this setting because those temperatures would not be known 14 days earlier when forecasts of 2AM temperatures are needed.

Leaning on the role of thermal inertia, the 2AM temperatures are fit as a bivariate time series with a loess smoother using only the 2PM fitted temperatures from 12 hours earlier as a precursor. Because the 2PM fitted values are a product of the predictor values two weeks before, they provide a bit of insight about forecasting performance with unlabeled data.<sup>2</sup>

In both plots, the relationship is approximately linear and positive with some hills and valleys. The local variation suggests that beyond a linear trend, there are some delimited processes pushing the fitted values up or down. They could be associated with reported heat waves, despite the previously mentioned definitional problems.

To the eye, the overall quality of the fit looks encouraging. Formal measures of fit for quantile regression have long been studied (Koenker and Machado, 1999), and based on equation 1, are easy to compute. But for this analysis of extreme values, overall fit can badly obscure fit quality for the relatively rare and extreme temperatures of interest. A good fit may result from the far more numerous lower temperatures that are of little concern. An alternative is provided below.

Partial dependence plots show that the relationships between the lagged predictors and the response variables are generally nonlinear. A plot of the influence of each predictor on the fitted values is dominated by the counter for day, but all of the lagged predictors contribute. Both additional displays of boosting results (Friedman, 2001, 2002) are a secondary concern because, again, an algorithm is not a model (Breiman, 2001). In the interest of space, those plots are not included.

#### 4.2.1 Fitted Values and Heat Waves

Returning to the interest of some researcher in reported heat waves, one might wonder how well the temperature fitted values correspond to any heat wave claims. Insofar as the fitted values reproduce credible heat wave reports, face validity of the approach taken might be enhanced. One useful technique simply is to display the same data responsible for Figure 2 reorganized to highlight trends over time. Figure 3 shows the result.

For both panels, the blue dots are the cases, the jagged blue line is the output from a loess smooth of the actual temperatures, and the jagged orange line is the output of a loess smooth of the fitted temperatures. The smoothed values again serve as a visual aid. The horizontal red line shows for each graph the value of the 90th percentile, which helps to put the plots in a useful context. The

---

<sup>2</sup>Most any widely used smoother such as regression splines could have been used and with proper tuning, the results would have been very similar. The loess span was set at .75 to help compensate for data sparsity around Q(.90) 2AM temperature values. Smaller spans ran without problems, but the fitted values were somewhat irregular and difficult to interpret visually.

dates of the reported heat wave shown in both panels were obtained from the Copernicus Climate Change Service of the European Union’s Copernicus Programme *after the full statistical analysis was completed.*

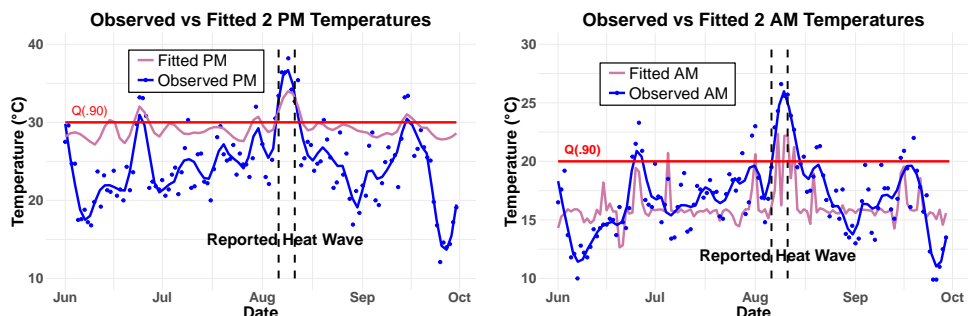


Figure 3: 2PM and 2AM results reorganized to display temporal trends. For readability, the graphed data include only June through September 2020. For both panels, the blue line is the loess smoothed observed temperature values, and the light orange line is the loess smoothed fitted values. The blue dots show the observed celsius temperatures. The red line is the  $Q(.90)$  for the observed temperatures. ( $N = 183$  days for 2PM and 181 Days for 2AM)

For Figure 3, cases for which the observed temperature exceeds the value of  $Q(.90)$  matter most. By construction, these are relatively rare. Starting with the left figure and the 2PM observed temperatures, the hills and valleys of the orange line tend to follow the hills and valleys of the blue line. Only one region contains a sequence of several days in which the  $Q(.90)$  values are exceeded. The largest spike for both the fitted 2PM temperatures and for the 2PM observed temperatures correspond quite well to one another, and quite well to the reported heat wave in the summer of 2020. The large orange spike, like all of the fitted values, is a product of the predictor variable values two weeks earlier. These results are comparable to the Paris diurnal results for 2019 in Berk (2025).

The results for 2AM are shown in the right panel. Again, both the largest blue spike and the largest orange spike correspond quite well to one another and also to the reported heat wave, although less definitively for the fitted values. Air temperatures at 2AM can be anticipated with fitted values from 2PM 12 hours earlier, derived, in turn, from predictors 14 days earlier using quantile gradient boosting and a loess smoother.

### 4.3 Forecasting and Uncertainty Estimates

Conformal prediction regions can provide provably valid coverage probabilities for forecasts of at least  $1 - \alpha$  for  $0 > \alpha < 1$ , specified before the forecasting analysis begins. The key requirement is that the observations used to construct the conformal prediction regions are exchangeable. One then can be certain with at least a probability of  $1 - \alpha$  that the true forecasted value will fall within the conformal prediction region conditional on the data and the algorithm used for training (Vovk et al., 2005, 2017; Angelopoulos et al., 2024). These are treated as fixed.

Multiple time series data will likely contain temporal dependence that undermines exchangeability. But if after fitting, the residuals are exchangeable, those residuals can be used as valid nonconformal scores. Adaptive conformal prediction regions can follow (Romano et al., 2019). Whether the residuals can be treated as exchangeable should be empirically addressed, not simply assumed.

The residuals produced when the quantile boosting algorithm was applied to the multiple time series data had temporal dependence for both the 2 PM and 2AM temperatures. After an AR(1) model was applied to those residuals, the new residuals were indistinguishable from white noise. The appended AR(1) model can be treated as a valid component of the training algorithm. White noise residuals imply exchangeability, and the residuals from the AR(1) model then can be valid nonconformal scores.

To obtain adaptive conformal prediction regions, quantile gradient boosting was applied to the 2PM nonconformal scores. However, the results were very unstable, and the fit often failed to improve after the first iteration. Quantile random forests was successfully substituted.<sup>3</sup> With white noise residuals, the data sampling essential for random forests does not create distortions in temporal dependence. There is no longer any temporal dependence to distort. Pseudocode is provided immediately below.

#### Pseudocode 1: Constructing 2PM Nonconformal Scores

**Input:** For time  $t = 1, \dots, T$ , let  $X_{t-14}$  denote the observed predictor values,  $y_t^{pm}$  denote the observed 2PM temperature,  $Q$  the target quantile for the algorithmic fit, and  $\alpha$  denote the value determining the  $1 - \alpha$  coverage probability.

Using  $Q$ , fit  $y_t^{pm}$  with  $X_{t-14}$  using the preferred machine learning algorithm such as quantile gradient boosting.

Compute fitted values  $\hat{y}_t^{pm} = \hat{y}^{pm}(\hat{y}_{t-14}^{pm})$ .

Compute the residuals  $r_t^{pm} = y_t^{pm} - \hat{y}_t^{pm}$ .

If  $r_t^{pm}$  has no temporal dependence,  $r_t^{pm}$  can serve as nonconformal scores.

If there is temporal dependence, fit a time series model to  $r_t^{pm}$  to account for serial correlation.

Let the white-noise residuals from the time series model be  $\epsilon_t^{pm}$ , which serve as the nonconformal scores.

Using the upper and lower bounds required by  $1 - \alpha$ , fit  $\epsilon_t^{pm}$  with  $y_t^{pm}$  using quantile random forests and save the resulting trained algorithm.

**Output:** Save the nonconformal scores, the trained quantile gradient boosting algorithm, and the trained quantile random forests algorithm for later use with a new unlabeled case.

<sup>3</sup>Quantile gradient boosting (QGB) directly minimizes a global quantile loss to estimate conditional quantile functions (Friedman, 2001), whereas quantile regression forests (QRF) uses variance-based splits within each tree and then recovers quantiles by post-processing the empirical distribution of responses in the leaves (Meinshausen, 2006). When the quantile estimation target is near the extremes, ensuing sparsity can derail QGB's loss minimization. Because QRF computes quantiles only after all trees in the forest are grown, such sparsity does not compromise the forest construction or ultimate results.

### Pseudocode 2: Forecasting 2PM Temperatures

**Input:** Let  $X_{T+1}^{pm}$  be the 14 day lagged predictor values for a new unlabeled case and  $1 - \alpha$  as the predetermined coverage probability.

Use the trained quantile gradient boosting algorithm to obtain the forecast  $\hat{y}_{T+1}^{pm} = \hat{y}(X_{T+1}^{pm})$  for two weeks in the future.

Using the trained quantile random forests with  $\hat{y}_{T+1}^{pm}$  as the predictor value, obtain the conformal upper and lower bounds for case  $T + 1$ .

Using the trained quantile random forest with  $\hat{y}_{T+1}^{pm}$  as the predictor value, extract the fitted values  $q_{T+1,\alpha/2}^{PM}$  and  $q_{T+1,1-\alpha/2}^{PM}$  as the lower and upper bound respectively of the prediction region at the desired coverage level  $1 - \alpha$ .

**Output:** Construct the prediction interval:

$$[\hat{y}_{T+1}^{pm} + q_{T+1,\alpha/2}^{PM}, \hat{y}_{T+1}^{pm} + q_{T+1,1-\alpha/2}^{PM}].$$

### Pseudocode 3: Constructing 2AM Nonconformal Scores

**Input:** As before, for time  $t = 1, \dots, T$ , let  $X_{t-14}$  denote the observed predictor values,  $y_t^{pm}$  denote the observed 2PM temperature,  $Q$  the target quantile for the algorithmic fit, and  $\alpha$  denote the value determining the  $1 - \alpha$  coverage probability.

As before, using  $Q$ , fit  $y_t^{pm}$  with  $X_{t-14}$  using the preferred machine learning algorithm such as quantile gradient boosting.

As before, compute fitted values  $\hat{y}_t^{pm} = \hat{y}^{pm}(\hat{y}_{t-14}^{pm})$ .

Fit a loess smoother using the one-day lagged predictor  $\hat{y}_{t-1}^{pm}$  and the response  $y_t^{am}$ , the observed 2 AM temperature.

Compute fitted values  $\hat{y}_t^{am} = \hat{y}^{am}(\hat{y}_{t-1}^{pm})$ .

Compute residuals  $r_t^{am} = y_t^{am} - \hat{y}_t^{am}$ .

If  $r_t^{am}$  has no temporal dependence,  $r_t^{am}$  can serve as nonconformal scores.

If there is temporal dependence, fit a time series model to  $r_t^{am}$  to account for serial correlation.

Let the white-noise residuals from the time series model be  $\epsilon_t^{am}$ , which serve as the nonconformal scores.

Fit quantile random forests to the nonconformal distribution  $\epsilon_t^{am}$  using  $\hat{y}_t^{am}$  as the predictor.

**Output:** Save the nonconformal scores, the trained quantile gradient boosting algorithm, and the trained quantile random forests algorithm for later use with a new unlabeled case, where  $X_{T+1}^{am}$  represents its 14 day lagged predictor values.

**Pseudocode 4: Forecasting 2AM Temperatures**

**Input:** Let  $X_{T+1}^{pm}$  be the 14 day lagged predictor values for a new unlabeled case. Use the fitted quantile gradient boosting algorithm to obtain  $\hat{y}_{T+1}^{pm} = \hat{y}^{pm}(X_{T+1}^{pm})$ . Insert  $\hat{y}_{T+1}^{pm}$  into the fitted loess smoother to obtain the forecast  $\hat{y}_{T+1}^{am} = \hat{y}^{am}(\hat{y}_{T+1}^{pm})$  for two weeks in the future. Insert  $\hat{y}_{T+1}^{am}$  into the fitted quantile random forest algorithm to obtain  $q_{T+1,\alpha/2}$  and  $q_{T+1,1-\alpha/2}$  required by  $1 - \alpha$ .

**Output:** Construct the prediction interval:

$$[\hat{y}_{T+1}^{am} + q_{T+1,\alpha/2}, \hat{y}_{T+1}^{am} + q_{T+1,1-\alpha/2}].$$

**4.3.1 A Sanity Check with Data from 2021**

A performance assessment of adaptive conformal prediction regions requires forecasts, in this case of 2PM and 2AM temperatures, because the length of the prediction regions depends in the forecasts. One can use the training data from 2020 for this purpose, but unreasonably optimistic results are likely. The forecasts are the fitted values from the training data.

A more realistic evaluation perhaps can be obtained for the 2021 data used earlier as test data. Its only earlier role was to provide information for a stopping rule for the quantile gradient boosting algorithm. The 2021 dataset has the same structure as the 2020 data one year later, and its predictors values can be used with the 2020 algorithmic results to obtain forecasts. An important advantage is that because in this case the true future temperatures have been observed, there is the prospect of an empirically based appraisal. The primary assumption is that the 2020 data and the 2021 data are realized in the same manner from the same population, joint probability distribution.

As before, extreme and rare high temperature are the focus. For illustrative purposes, Table 1 shows some conformal results for the highest 10% of the forecasted 2PM and 2AM temperatures respectively for 2021. These are the temperatures likely to be of greatest subject-matter and policy interest and are produced from 2021 predictor values 14 days earlier. As expected, one can see that the prediction regions are more precise (i.e., shorter) for  $1 - \alpha = .70$  than for  $1 - \alpha = .90$ .

More precise predictions arguably imply a better fit. The average length of the prediction region depends on the variability the data, the fitting performance of the forecasting algorithm, and the specified coverage probability, as well as more technical matters such as what kind of nonconformal score is used (Gupta et al., 2022; Adams et al., 2024). Conventional regression measures of fit at least implicitly condition in analogous ways.

The top row in Table 1 shows the minimum, mean and maximum prediction regions for  $1 - \alpha = .90$  and  $1 - \alpha = .70$ . The values seem uncomfortably large perhaps until one considers that the prediction region length is split so that one part falls below the forecasted 2PM temperature, and the other part falls above. On the average, that is about  $\pm 4^\circ\text{C}$  for the larger coverage probability and a little less than  $\pm 3^\circ\text{C}$  for the smaller coverage probably. From a practical perspective, moreover, all a policy maker might care about is the probability that the future true 2PM temperature falls above the lower bound. For example, if the forecast is  $30^\circ\text{C}$  and the length of the prediction region

Table 1: In celsius degree units, the minimum, mean, and maximum adaptive prediction region lengths for the top 10% of the of the 2021 forecasted 2PM and 2AM temperatures for  $1 - \alpha = .90$  or  $.70$ .

Time	Min .90	Mean .90	Max .90	Min .70	Mean .70	Max .70
2PM	6.5	8.2	10.4	4.1	5.6	8.5
2AM	1.0	3.8	5.3	1.0	3.4	5.1

is  $\pm 3^\circ\text{C}$  for the  $.70$  coverage probability, the probability that the true 2PM temperature 14 days later will be greater than  $27^\circ\text{C}$  is  $.85$ . More is said about this use of conformal prediction regions shortly.

The same interpretive strategy can be used for the 2AM temperatures in the bottom row of Table 1. The 2AM forecasts are more precise than the 2PM forecasts, in part because there is less variability of the 2AM temperatures. As before, a lower coverage probability generally improves precision. For  $1 - \alpha = .90$ , the average length of the adaptive prediction region is a little less than  $\pm 2^\circ\text{C}$ . For  $1 - \alpha = .70$ , the average length of the adaptive prediction region is a little more than  $\pm 1.5^\circ\text{C}$ . The lower bound rationale also works as before. Whether the precision performance in Table 1 is adequate overall should be a decision made by stakeholders. There is the option of using a value of  $1 - \alpha$  that is smaller than  $.70$ , and the coverage tradeoff for greater precision remains.<sup>4</sup>

## 5 Discussion

The empirical results and statistical methods used in this paper seem to have promise for projections two weeks in advance of high and rare temperatures, whether in the heat of the day or the heat of the following night. The approach relies on weather station data available worldwide, easily accessible through NOAA, simply curated as csv files, and free. Routine machine learning algorithms available in R and python are used that can be executed on a standard desktop computer with very modest amounts of tuning. Given the trained algorithm and its training data, provably valid estimates of uncertainty can be provided.

An important concern is whether the methods used with the Paris data will perform well elsewhere. Paris is proximate to the Loire Vally. It has a temperate oceanic climate coupled with urban heat island effects. The winters are mild and the summers are warm. Cloud cover is common, and humidity is moderate. Rain falls evenly throughout the year. There are many areas around the globe that properly could be described in a similar manner. Challenging would be locales where the climate is very different such as the American Southwest (e.g., Phoenix), sites near the Arctic Circle (e.g., Fairbanks), and the African Mediterranean coast (e.g., Algiers). There likely are several cluster of locations that are each sufficiently similar, but statistical adjustments likely are necessary

---

<sup>4</sup>One can examine a range of precisions by trying a range of  $1 - \alpha$  values, but then one is engaged in post selection inference and a simultaneous coverage method is required (Sarkar and Kuchibhotla, 2023). A variant on the usual Bonferroni method is valid, but conservative. Some precision is lost.

across these clusters. It is a lot to ask one massive algorithm to accurately forecast excessive heat for very different settings whereas lots of small studies might succeed.

There also are issues of statistical robustness. Are the results relatively stable with longer or shorter predictor lags or different kinds of test data? Might it be useful to pool data from several proximate weather stations or build in predictor information from weather stations that are not near one another but in the direction from which weather systems usually arrive. Is the  $Q(.90)$  fitting target ideal? A  $Q(.95)$  fitting target might lead to very sparse high temperature data, while a  $Q(.80)$  fitting target might include too many temperatures that are not sufficiently extreme. Relevant factors would be the sample size and temperature distributions.

How the nonconformal scores are used in practice warrants additional thought. Policy makers may be more interested in whether forecasted temperatures exceed some hazard threshold than in the length of the prediction region. Suppose there is public health research showing that for a particular locale temperatures above  $32^{\circ}\text{C}$  are associated with a dramatic increase in emergency room admission for hyperthermia.<sup>5</sup> Then it might be useful to know whether that temperature falls above the lower bound of the prediction interval. Another application would be to allow decision makers to examine a range of tradeoffs between coverage and precision. There is unlikely to be an a priori and compelling value for either the coverage probability or for precision. Consequently, a reasonable approach might be to specify a range of values for  $1 - \alpha$  for which different precision could be evaluated, and an empirically informed, preferred tradeoff selected. Sarkar and Kuchibhotla (2023) show how such a search can invalidate conventional conformal prediction regions, and what can be done to fix the problem.

If the methods in this paper prove sufficiently effective, there might be important implications for heat wave preparedness. With a 14 day lead time, a range of proactive measures could be implemented or at least better planned. Examples include checking on elderly individuals living alone, preparation of cooling buildings that can be used as refuges, proper staffing and provisioning of hospital emergency rooms, and having fire fighters and supporting equipment moved near undeveloped land vulnerable to wild fires.

Finally, for the work in this paper to be useful, it must be more than a one-off. There are thousands of geographically dispersed weather stations producing data having comparable content and structure. Even most of the variable names are the same. In the medium term at least, one can envision ensembles of applications organized by local climate. But for local policy purposes, separate applications for each location might be necessary.

## 6 Conclusions

There are no doubt possible improvements to the methods employed here. They would likely require a lengthy methodological discussion beyond the intent and scope of this paper. But perhaps a foundation has been laid. It seems possible to forecast rare and high temperatures two weeks in advance with useful accuracy. The requisite data is easily obtained. The analyses can be undertaken

---

<sup>5</sup>This will depend on local cooling technology, its prevalence, and housing arrangements, not just temperatures and humidity.

on a laptop or desktop computer equipped with python or R. Valid measure of uncertainty are readily computed. Forecasts of extreme heat may not always require industrial strength procedures.

## References

- J.R. Adams, B. Berman, D. Rina, and J.J. Michalenko. Non-conformity scores for high-quality uncertainty quantification from conformal prediction. Technical Report SAND-2023-10422R, Sandia National Laboratories, Albuquerque, NM, 2024. URL <https://doi.org/10.2172/2430248>.
- G. B. Anderson and M. L. Bell. Weather-related mortality: How heat, cold, and heat waves affect mortality in the united states. *Epidemiology*, 20(2):205–213, 2009. doi: 10.1097/EDE.0b013e318190ee08.
- A. N. Angelopoulos, R. F. Barber, and S. Bates. Theoretical foundations of conformal prediction, 2024. URL <https://arxiv.org/abs/2411.11824>. Preprint; forthcoming with Cambridge University Press.
- R. A. Berk. Forecasting extreme high summer temperatures in paris and cairo using gradient boosting and conformal prediction regions, 2025. URL <https://arxiv.org/abs/2506.02349>.
- C. Bodnar, W. P. Bruinsma, A. Lucic, et al. A foundation model for the earth system. *Nature*, 641:1180–1187, 2025. doi: 10.1038/s41586-025-09005-y.
- L. Breiman. Statistical modeling: The two cultures. *Statistical Science*, 16(3):199–231, 2001. doi: 10.1214/ss/1009213726. URL <https://doi.org/10.1214/ss/1009213726>.
- T. Elsken, J. H. Metzen, and F. Hutter. Neural architecture search. In F. Hutter, L. Kotthoff, and J. Vanschoren, editors, *Automated Machine Learning*, pages 63–77. Springer, Cham, 2019. doi: 10.1007/978-3-030-05318-5\_3. URL [https://doi.org/10.1007/978-3-030-05318-5\\_3](https://doi.org/10.1007/978-3-030-05318-5_3).
- J. H. Friedman. Greedy function approximation: A gradient boosting machine. *The Annals of Statistics*, 29(5):1189–1232, 2001. doi: 10.1214/aos/1013203451. URL <https://doi.org/10.1214/aos/1013203451>.
- J. H. Friedman. Stochastic gradient boosting. *Computational Statistics & Data Analysis*, 38(4):367–378, 2002. doi: 10.1016/S0167-9473(01)00065-2. URL [https://doi.org/10.1016/S0167-9473\(01\)00065-2](https://doi.org/10.1016/S0167-9473(01)00065-2).
- B. Fu. State of the science fact sheet: Uncertainty in forecasting weather and water. Technical Report 69977, National Oceanic and Atmospheric Administration, 2025. URL <https://doi.org/10.25923/3r83-dt50>.
- E. Galván and P. Mooney. Neuroevolution in deep neural networks: Current trends and future challenges. *IEEE Transactions on Artificial Intelligence*, 2(6):476–493, 2021. doi: 10.1109/TAI.2021.3067574. URL <https://doi.org/10.1109/TAI.2021.3067574>.
- A. Gettleman and R. B. Rood. *Demystifying Climate Models: A User’s Guide to Earth System Models*. Springer Praxis Books. Springer, Cham, 2016. doi: 10.1007/978-3-662-52838-0. URL <https://doi.org/10.1007/978-3-662-52838-0>.
- S. O. Guimarães, M. E. Mann, S. Rahmstorf, et al. Increased projected changes in quasi-resonant amplification and persistent summer weather extremes in the latest multimodel cli-

- mate projections. *Scientific Reports*, 14:21991, 2024. doi: 10.1038/s41598-024-72787-0. URL <https://doi.org/10.1038/s41598-024-72787-0>.
- C. Gupta, A.K. Kuchibhotla, and A. Ramdas. Nested conformal prediction and quantile out-of-bag ensemble methods. *Pattern Recognition*, 127:0031–3203, 2022. doi: <https://doi.org/10.1016/j.patcog.2021.108496>. URL <https://www.sciencedirect.com/science/article/pii/S0031320321006725>.
- K. Harper. The history of synoptic meteorology in the age of numerical weather forecasting. In *Oxford Research Encyclopedia of Environmental Science*. Oxford University Press, 2024. doi: 10.1093/acrefore/9780199389414.013.774. URL <https://doi.org/10.1093/acrefore/9780199389414.013.774>.
- C. He, H. Kim, M. Hashizume, et al. The effects of night-time warming on mortality burden under future climate change scenarios: A modeling study. *The Lancet Planetary Health*, 6(8):e648–e657, 2022. doi: 10.1016/S2542-5196(22)00139-5. URL [https://doi.org/10.1016/S2542-5196\(22\)00139-5](https://doi.org/10.1016/S2542-5196(22)00139-5).
- J.E. Hopke. Connecting extreme heat events to climate change: Media coverage of heat waves and wildfires. *Environmental Communication*, 14(4):492–508, 2020. doi: 10.1080/17524032.2019.1687537. URL <https://doi.org/10.1080/17524032.2019.1687537>.
- M. Hulme, S. Dassai, I. Lorenzoni, and D.R. Nelson. Unstable climates: Exploring the statistical and social constructions of 'normal' climate. *Geoforum*, 40:197–205, 2008. doi: 10.1016/j.geoforum.2008.09.010. URL <https://doi.org/10.1016/j.geoforum.2008.09.010>.
- R.J. Hyndman and G. Athanasopoulos. *Forecasting: Principles and Practice*. OTexts, Melbourne, 3 edition, 2021. URL <https://otexts.com/fpp3/>.
- IPCC. Summary for policymakers. In H. Lee and J. Romero, editors, *Climate Change 2023: Synthesis Report. Contribution of Working Groups I, II and III to the Sixth Assessment Report of the Intergovernmental Panel on Climate Change*, pages 1–34. IPCC, Geneva, 2023. doi: 10.59327/IPCC/AR6-9789291691647.001. URL <https://www.ipcc.ch/report/ar6/syr/summary-for-policymakers/>.
- V. Jacques-Dumas, F. Ragone, P. Borgnat, P. Abry, and F. Bouchet. Deep learning-based extreme heatwave forecast. *Frontiers in Climate*, 4:789641, 2022. doi: 10.3389/fclim.2022.789641. URL <https://doi.org/10.3389/fclim.2022.789641>.
- M. Kearns and A Roth. *The Ethical Algorithm: The Science of Socially Aware Algorithm Design*. Oxford University Press, New York, 2019.
- D. Klingelhöfer, M. Braun, D. Brueggmann, and D.A. Groneberg. Heatwaves: Does global research reflect the growing threat in the light of climate change? *Globalization and Health*, 19:56, 2023. doi: 10.1186/s12992-023-00955-4. URL <https://doi.org/10.1186/s12992-023-00955-4>.
- R. Koenker and J.A.F. Machado. Goodness of fit and related inference processes for quantile regression. *Journal of the American Statistical Association*, 94(448):1296–1310, 1999. doi: 10.1080/01621459.1999.10473882. URL <https://doi.org/10.1080/01621459.1999.10473882>.
- X. Li, M.E. Mann, M.F. Wehner, et al. Role of atmospheric resonance and land–atmosphere feedbacks as a precursor to the june 2021 pacific northwest heat dome event. *Proceedings of the National Academy of Sciences*, 121(4):e2315330121, 2024. doi: 10.1073/pnas.2315330121. URL

- <https://doi.org/10.1073/pnas.2315330121>.
- M.E. Mann, S. Rahmstorf, K. Kornhuber, and B.A. Steinman. Projected changes in persistent extreme summer weather events: The role of quasi-resonant amplification. *Science Advances*, 4(10):eaat3272, 2018. doi: 10.1126/sciadv.aat3272. URL <https://doi.org/10.1126/sciadv.aat3272>.
- C.F. Manski and S.R. Lerman. The estimation of choice probabilities from choice based samples. *Econometrica*, 45(8):1977–1988, 1977. URL <https://doi.org/10.2307/1914121>.
- W. Marx, R. Aunshild, and L. Bornmann. Heat waves: A hot topic in climate change research. *Theoretical and Applied Climatology*, 146:781–800, 2021. doi: 10.1007/s00704-021-03758-y. URL <https://doi.org/10.1007/s00704-021-03758-y>.
- K.A. McKinnon and I.R. Simpson. How unexpected was the 2021 pacific northwest heatwave? *Geophysical Research Letters*, 49(18), 2022. doi: 10.1029/2022GL100380. URL <https://doi.org/10.1029/2022GL100380>.
- N. Meinshausen. Quantile regression forests. *Journal of Machine Learning Research*, 7:983–999, 2006. URL <http://www.jmlr.org/papers/v7/meinshausen06a.html>.
- G. Miloshevich, D. Lucente, P. Yiou, and F. Bouchet. Extreme heat wave sampling and prediction with analog markov chain and comparisons with deep learning. *Environmental Data Science*, 3:e9, 2024. doi: 10.1017/eds.2024.7. URL <https://doi.org/10.1017/eds.2024.7>.
- S.E. Perkins. A review on the scientific understanding of heatwaves — their measurement, driving mechanisms, and changes at the global scale. *Atmospheric Research*, 165:242–267, 2015. doi: 10.1016/j.atmosres.2015.05.014. URL <https://doi.org/10.1016/j.atmosres.2015.05.014>.
- S.E. Perkins and L.V. Alexander. On the measurement of heat waves. *Journal of Climate*, 26(13):4500–4517, 2013. doi: 10.1175/JCLI-D-12-00383.1. URL <https://doi.org/10.1175/JCLI-D-12-00383.1>.
- V. Petoukhov, S. Rahmstorf, S. Petri, and H.J. Schellnhuber. Quasiresonant amplification of planetary waves and recent northern hemisphere weather extremes. *Proceedings of the National Academy of Sciences*, 110(14):5336–5341, 2013. doi: 10.1073/pnas.1222000110. URL <https://doi.org/10.1073/pnas.1222000110>.
- A. Piticar, S. Cheval, and M. Frighenciu. A review of recent studies on heat wave definitions, mechanisms, changes, and impact on mortality. *Forum Geographic*, 18(2):103–120, 2019. doi: 10.5775/fg.2019.019.d. URL <http://dx.doi.org/10.5775/fg.2019.019.d>.
- C. Porter. Paris braces for a future of possibly paralyzing heat. *The New York Times*, August 2025. URL <https://www.nytimes.com/2025/08/18/world/europe/france-heat-wave-paris-climate-change-planning.html>.
- I. Price, A. Sanchez-Gonzalez, F. Alet, et al. Probabilistic weather forecasting with machine learning. *Nature*, 624:559–563, 2024. doi: 10.1038/s41586-024-08252-9. URL <https://doi.org/10.1038/s41586-024-08252-9>. Accessed 18 August 2025.
- Z. Pu and E. Kalnay. Numerical weather prediction basics: Models, numerical methods, and data assimilation. In Q. Duan, F. Pappenberger, J. Thielen, A. Wood, H. Cloke, and J. Schaake, editors, *Handbook of Hydrometeorological Ensemble Forecasting*, pages 67–97. Springer, Berlin, Heidelberg, 2018. URL <https://link.springer.com/book/10.1007/978-3-642-39925-1>.

- Y. Romano, E. Patterson, and E.J. Candès. Conformalized quantile regression. In H. Wallach et al., editors, *Advances in Neural Information Processing Systems 32 (NeurIPS 2019)*, volume 32, 2019. URL <https://papers.neurips.cc/paper/8613-conformalized-quantile-regression.pdf>.
- L.P. Rothfus. The heat index equation (or, more than you ever wanted to know about heat index). Technical Report SR 90-23, National Weather Service, Southern Region Headquarters, Fort Worth, TX, 1990. URL [https://www.weather.gov/media/ffc/ta\\_htindx.PDF](https://www.weather.gov/media/ffc/ta_htindx.PDF). Scientific Services Division Technical Attachment.
- S. Sarkar and A.K. Kuchibhotla. Post-selection inference for conformal prediction: Trading off coverage for precision, 2023. URL <https://doi.org/10.48550/arXiv.2304.06158>.
- S.H. Schneider. The greenhouse effect: Science and policy. *Science*, 243(4892):771–781, 1989. doi: 10.1126/science.243.4892.771. URL <https://doi.org/10.1126/science.243.4892.771>.
- T.T. Smith, B.F. Zaitchik, and J.M. Gohlke. Heat waves in the united states: Definitions, patterns and trends. *Climatic Change*, 118:811–825, 2013. doi: 10.1007/s10584-012-0659-2. URL <https://doi.org/10.1007/s10584-012-0659-2>.
- R.G. Steadman. The assessment of sultriness. part i: A temperature-humidity index based on human physiology and clothing science. *Journal of Applied Meteorology*, 18(7):861–873, 1979. doi: 10.1175/1520-0450(1979)018<0861:TAOSPI>2.0.CO;2. URL [https://doi.org/10.1175/1520-0450\(1979\)018<0861:TAOSPI>2.0.CO;2](https://doi.org/10.1175/1520-0450(1979)018<0861:TAOSPI>2.0.CO;2).
- R. Stull. *Practical Meteorology: An Algebra-Based Survey of Atmospheric Science*. University of British Columbia Press, 2017. URL [https://www.eoas.ubc.ca/books/Practical\\_Meteorology/](https://www.eoas.ubc.ca/books/Practical_Meteorology/).
- E. Tziperman. *Global Warming Science*. Princeton University Press, 2022.
- J. Velthoen, C. Dombry, J.J. Cai, and S. Engelke. Gradient boosting for extreme quantile regression. *Extremes*, 26:639–667, 2023. doi: 10.1007/s10687-023-00473-x. URL <https://doi.org/10.1007/s10687-023-00473-x>.
- V. Vovk, A. Gammerman, and G. Shafer. *Algorithmic Learning in a Random World*. Springer, New York, 2005.
- V. Vovk, J. Shen, V. Manokhin, and M. Xie. Nonparametric predictive distributions based on conformal prediction. *Proceedings of Machine Learning Research*, 69:82–102, 2017.
- G.-R. Walther, E. Post, P. Convey, et al. Ecological responses to recent climate change. *Nature*, 416(689):389–395, 2002. doi: 10.1038/416389a. URL <https://doi.org/10.1038/416389a>.
- F. Wang, D. Tian, L. Lowe, L. Katlin, and J. Lehrter. Deep learning for daily precipitation and temperature downscaling. *Water Resources Research*, 57(8):e2020WR029308, 2021. doi: 10.1029/2020WR029308. URL <https://doi.org/10.1029/2020WR029308>.